Chapter 5

Dynamics of membrane adhesion mediated by receptor interactions

5.1 Introduction

Cell adhesion is crucial to many biological processes, including cell differentiation and division, signal transduction, and immunological responses (Alberts et al., 2002; Berg et al., 2002; Springer, 1990). Many different interactions are involved in adhesions *in vivo*: lock-and-key type interactions between proteins (Lauffenburger and Linderman, 1993), force-induced signaling, reorganization of actin filaments and the cortex (Lipowsky, 1995), and various generic physical forces (Nelson et al., 2004). Despite the complexity of these interactions, researchers have been successful in explaining many experimental observations from thermodynamic and physico-chemical analysis, and many features of cell adhesion can be qualitatively understood from basic physical principles (Bell, 1978; Bell et al., 1984; Torney et al., 1986; Coombs et al., 2004; Flyvbjerg et al., 1997; Zukerman and Bruinsma, 1995; Lipowsky, 1996; Bruinsma et al., 2000; Boulbitch et al., 2001; Bruinsma and Sackmann, 2002; Sackmann and Bruinsma, 2002; Sackmann and Goennenwein, 2006).

In contrast to adhesion mediated by generic interactions such as the van der Waals or electrostatic forces, biological adhesions are induced by specific binding between proteins with complementary domains, i.e, receptors and ligands. Other interactions provide different regulation mechanisms to fortify (e.g., cytoskeleton reorganization) or destabilize (e.g., repeller molecules) the adhesion contact. While adhesion receptors play the major role and are extensively studied, de-adhesion forces are crucial to ensure *specificity* of the adhesion (Bruinsma et al., 2000; Bruinsma and Sackmann, 2002). The interplay between attractive specific and (usually repulsive) non-specific forces is a recurring theme in cell adhesion, and provides delicate control over the adhesion–de-adhesion process in cell migration and immunological response.

While receptors and their ligands have been the focus of biological studies over the past decades, the physical carrier of these proteins—the cell membrane—has been extensively studied by physicists and biophysicists since the fluid-mosaic model was proposed by Mitchell and Nicholson. Membranes are composed of self-assembled lipid molecules and form vesicles in aqueous solutions of typical sizes up to 10 μm. The physics of fluid or solid membranes are well studied and summarized by Peliti (1994), Nelson et al. (2004), and Safran (1994). In particular the interactions between flexible membranes have been studied by Lipowsky and co-workers (Peliti and Leibler, 1985; Lipowsky and Leibler, 1986; Lipowsky, 1994, 1995).

Recent advances in bioengineering techniques have enabled studies of adhesion between biomimetic membranes mediated by specific and non-specific interactions. Sackmann and co-workers (Sackmann, 1996; Tanaka and Sackmann, 2005) have designed self-assembled vesicles and monolayers supported by a polymer cushion to mimic cell membranes and the extracellular matrix; in the membranes they incorporated specific proteins (to mimic ligand-receptor binding), glycolipids (to mimic the glycocalyx), as well as other additives to stabilize the vesicles. This system provides the first

biomimetic system incorporating key elements in cell adhesion and allows systematic studies of the dynamics and mechanics of adhesion without complications due to other factors present in biological cells.

Based on *in vitro* experiments using biomimetic vesicles, Sackmann, Bruinsma, and co-workers (Bruinsma et al., 2000; Bruinsma and Sackmann, 2002; Sackmann and Goennenwein, 2006) found that cell adhesion is controlled by a double-well potential: a weak-adhesion state at a large surface separation due to generic van der Waals interactions between lipids, and a strong-adhesion state at a small surface separation due to ligand-receptor binding; membrane undulation and glycolipid depletion induce repulsive forces that constitute the barrier between the two minima. The adhesion process proceeds in three steps (Albersdörfer et al., 1997; Kloboucek et al., 1999; Boulbitch et al., 2001; Sackmann and Bruinsma, 2002). First, small adhesion contacts are formed which are most likely induced by membrane undulations; such a process is an activated process with a nucleation barrier larger than 10 $k_{\rm B}T$. Following nucleation, receptors diffuse into the adhesion contacts and contact area grows accompanied by a depletion of repellers (glycolipids), this is the growth step. Finally, after receptors are depleted, the adhesion contacts evolve like coarsening in a phase separation: the number of adhesion contacts decreases and various small focal contacts are formed with high densities of receptors, accompanied by a possible decrease in the total area of contact. The whole process is likened to the wetting transition (Bruinsma and Sackmann, 2002) and phenomenological parameters like the surface tension, the spreading pressure, and the contact angle can be measured and related to underlying parameters, including the mechanical properties of the membrane and the molecular parameters of receptors (Bruinsma et al., 2000; Simson et al., 1998; Boulbitch et al., 2001).

The conformations of adhered membranes are recorded *in situ* by reflection interference contrast microscopy (RICM) (Rädler and Sackmann, 1993; Rädler et al., 1995), which provide direct experimental measurements of the formation and growth of adhesion plaques. However, RICM is unable to resolve adhesion contacts smaller than 300 nm (Boulbitch et al., 2001), therefore cannot give direct support for the nucleation process. On the other hand, scaling arguments and Monte Carlo studies (Lipowsky, 1994; Volmer et al., 1998) usually cannot yield quantitative results that are experimentally testable.

In this paper we present a systematic study of the nucleation step of the adhesion controlled by a double-well interacting potential. Following Bruinsma et al. (2000), Bruinsma and Sackmann (2002), and Sackmann and Bruinsma (2002), we assume the "minimum" model of membrane adhesion consisting of the elastic deformation energy of the flexible membrane and the double-well adhesion potential. As discussed above, this minimum model preserves the key features of cell adhesion. From a scaling analysis we find that the membrane shapes are governed by the adhesion length R_0 which is determined from the bending rigidity κ and adhesion potential; the energy barrier is controlled

by the energy scale $\sqrt{\kappa V_{\rm eff} L_0^2}$, where $V_{\rm eff}$ is the effective barrier height and L_0 is the characteristic length determined by the adhesion potential.

If $F_0 \gg k_{\rm B}T$, adhesion is a first-order transition and nucleation proceeds along the "minimum energy path" governed by the effective potential (free energy). Using the string method by E et al. (2002), we calculate the "minimum energy path" from the weakly bound state to a well-developed adhesion contact. We find that the typical energy barrier for adhesion between flexible membranes is about 20–30 $k_{\rm B}T$, corresponding to a time scale of 0.1–1000 seconds. For adhesion of cells with actin cortices, which have much larger bending modulus, the nucleation barrier is much larger and is essentially insurmountable by thermal undulations, and actin reorganization and cell signaling provide additional mechanisms for stabilizing the adhesion contact.

For F_0 comparable to $k_{\rm B}T$, we adopt a Peierls argument following Lipowsky (1994, 1995). We find that near the critical unbinding transition, adhesion is a weak first-order transition, and the adhesion dynamics depend on the shape of the irregular boundary. We show that if the potential minima have comparable depth, the adhesion dynamics are controlled by the potential depths only, and independent of the length scale of the double-well potential, which reflects the dominance of membrane undulations.

5.2 Model and solution

5.2.1 Model description

The thickness of a self-assembled monolayer or bilayer is about 10–100 nm, thus negligible compared to the spatial extension (~ 10 μm). Therefore the macroscopic behaviors of membranes are mostly determined by their geometric shapes, and to a good approximation independent of the microscopic degrees of freedom of the consistituent amphiphilic molecules. Flexible membranes as random surfaces have been extensively studied in the past decades by physicists; theoretical models and results are collected in the book edited by Nelson et al. (2004). For cell membranes or self-assembled monolayers with biological relevance, see Safran (1994) and the book edited by Lipowsky (1995); a more up-to-date review of simulation methods and other approaches is given by Müller et al. (2006).

For a single membrane that is homogeneous, smooth, and non-interacting, Canham (1970) and Helfrich (1973) proposed that up to 2nd-order derivatives with respect to the local coordinates of the membrane shape, the elastic energy of a deformed membrane is given by

$$\frac{H_{\rm e}}{k_{\rm B}T} = \int_S \left[\sigma + \frac{1}{2}\kappa \left(H - H_0\right)^2 + \bar{\kappa} K\right] {\rm d}A. \tag{5.1}$$

Here σ is the (local) surface tension conjugate to the surface area, κ and $\bar{\kappa}$ are elastic moduli known as the bending regidity and the Gaussian rigidity coupled to the mean curvature H and the Gaussian

curvature K, H_0 is the spontaneous curvature. The integral is over the whole membrane area[1].

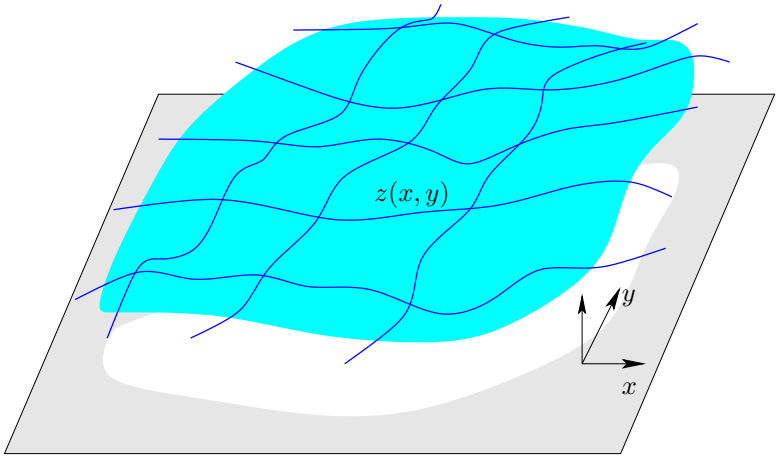

Figure 5.1: Monge representation of a near-flat membrane shape

In this paper we study the adhesion between a flexible membrane and a flat surface, corresponding to the experimental system studied by Bruinsma et al. (2000). For this model the separation between the membrane and the flat surface provides a natural representation of the membrane shape (cf. Fig. 5.1), $z = z(x, y)$, also called the Monge representation[2]. Since we focus on the initial stage of adhesion where the adhesion contact is small compared to the size of the membrane, we assume $H_0 = 0$, and in this case the Monge representation is useful. The elastic energy of the membrane is given by

$$\frac{H_\mathrm{e}}{k_\mathrm{B}T} = \int \left\{ \frac{\kappa}{2} \left[\Delta z(x, y)\right]^2 + \sigma \left[\nabla z(x, y)\right]^2 \right\} \mathrm{d}x\mathrm{d}y. \tag{5.2}$$

The elastic energy gives the "kinetic" part of the Hamiltonian, now we consider the interacting potential between the membrane and the adhering surface. Generic (non-specific) interactions, including the van der Waals interaction, electrostatic interaction, and hydration forces (see Nelson et al., 2004, Chapter 3) results in a potential V_g with a minimum around 10–100 nm (Albersdörfer et al., 1997; Bruinsma et al., 2000; Guttenberg et al., 2001). The net interaction between the surfaces mediated by receptors and repellers has been calculated in our previous paper[3]; for phenomenological treatments, see Zukerman and Bruinsma (1995), Bruinsma et al. (2000), and Weikl et al. (2002).

[1] The Helfrich Hamiltonian is the simplest renormalizable model for fluctuating membranes that satisfies Euclidean symmetry and reparametrization invariance; the functional accounts for the energy of elastic deformations from the equilibrium state with minimum area A_min and uniform curvature H_0. If the Gaussian rigidity is constant, then the Gaussian curvature term is constant for a surface with fixed topology (Euler characteristic). See Peliti (1994) and Nelson et al. (2004) for thorough discussions.

[2] In the case of adhesion between two membranes, the elastic energy is divided into two parts: one due to deformation of the "center of mass" of the binary system, the other dependent on the relative separation between the membranes; after integrating out the center of mass deformations, one can write the elastic energy dependent on the relative separation in the same form as above with the additive bending rigidity (cf. Lipowsky (1996))

$$\kappa^{-1} = \kappa_1^{-1} + \kappa_2^{-1}.$$

[3] Manuscript submitted to *Langmuir*.

The interaction potential due to receptors $V_{\rm s}$ can be generally written as a functional of the density distributions $\phi_{\rm i}(x,y)$, and $\phi_{\rm i}$ depends on the local surface separation $z(x,y)$. Here we assume that molecular transport is fast enough so that we can write $V_{\rm s}$ as a functional of the separation $z(x,y)$. Therefore the total Hamiltonian is given by [$\mathbf{r}=(x,y)$]

$$H[z(\mathbf{r}),\phi_{\rm i}(\mathbf{r})] = H_{\rm e}[z(\mathbf{r})] + V_{\rm g}[z(\mathbf{r})] + V_{\rm s}[z(\mathbf{r})]. \tag{5.3}$$

The free energy (effective potential) of the model given by (5.3) can be calculated by standard field theoretic method by integrating out fluctuations of the separation variable $z(\mathbf{r})$. These fluctuation effects have been extensively studied (Nelson et al., 2004); in particular, membrane fluctuations induce an effective repulsion which contributes to $V[z(\mathbf{r})]$. Since fluctuation effects are not our focus here, we apply a mean-field approximation and assume the free energy takes the same form as the Hamiltonian with *renormalized* elastic constants and interacting potential: these renormalized parameters are experimentally measurable; we shall consider the membrane undulation effects in Section 5.4 by scaling arguments.

With these approximations we can write the effective potential of our model as

$$\frac{F[z(\mathbf{r})]}{k_{\rm B}T} = \int \left\{ \frac{\kappa}{2} \left[\Delta z(\mathbf{r})\right]^2 + \sigma \left[\nabla z(\mathbf{r})\right]^2 + V[z(\mathbf{r})] \right\} {\rm d}^2\mathbf{r}. \tag{5.4}$$

The adhesion (interacting) potential $V(z)$ has a double-well shape (Bruinsma et al., 2000; Bruinsma and Sackmann, 2002) and is characterized by the depths of and the locations of the minima, as is schematically shown in Fig. 5.2(a). The parameters in Eq. (5.4) have been measured by Sackmann and co-workers in different systems (see Flyvbjerg et al., 1997; Simson et al., 1998; Kloboucek et al., 1999; Bruinsma and Sackmann, 2002; Sackmann, 2006; Sackmann and Goennenwein, 2006). κ is about 20 $k_{\rm B}T$ for a self-assembled bilayer, and of order 1000 $k_{\rm B}T$ for cells with actin cortices. σ is related to the so-called capillary length (Sackmann and Goennenwein, 2006)

$$R_{\rm c} = \sqrt{\kappa/\sigma},$$

which defines the length scale above which surface tension becomes important. Typical values for $R_{\rm c}$ are about 0.1–1 μm (Bruinsma et al., 2000; Sackmann and Goennenwein, 2006). Generally the size of adhesion plaques in the initial stage of adhesion is smaller than $R_{\rm c}$, therefore the bending energy dominates.

For clarity of our discussion it is convenient to scale the separation $z(\mathbf{r})$ and the radial coordinate r by natural length scales arisen from the adhesion potential and the membrane elasticity. After the general rescaling

$$r/R_0 \to r,\ l/L_0 \to l,\ z/L_0 \to z; V/V_2 \to v$$

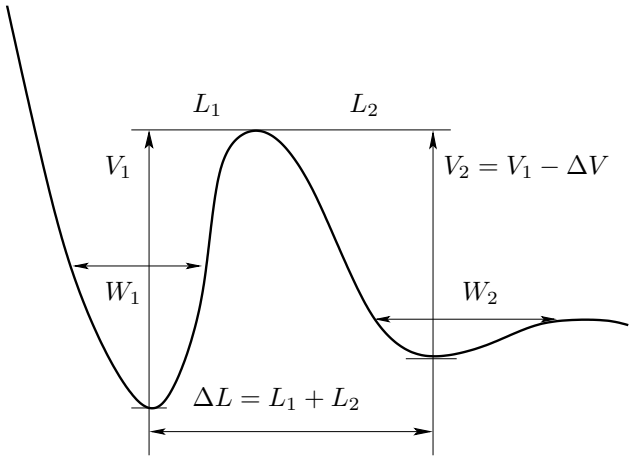

Figure 5.2: Schematic representation of the interaction potential $V(z)$. The shape of the potential is similar to that calculated from a phenomenological model proposed by Bruinsma et al. (2000). Only the part of the potential inbetween the minima are important for our calculations, and the potential is characterized by the position L_1, L_2 (fixing the barrier at the origin) and the depths W_1, W_2 of the minima. In our numerical calculations we choose the functional form for $V(z)$ such that the widths $W_1 \approx L_1$ and $W_2 \approx L_2$ for fast convergence.

the effective potential becomes

$$\frac{F[z]}{k_\mathrm{B}T} = \int_S \left[\frac{\kappa L_0^2}{2R_0^2}\left(\nabla^2 z\right)^2 + \gamma L_0^2 \left(\nabla z\right)^2 + V_2 R_0^2 v(z)\right] \mathrm{d}^2\mathbf{r}. \tag{5.5}$$

In the rigidity dominant regime, we choose

$$V_2 R_0^2 = \frac{\kappa L_0^2}{R_0^2},$$

such that the length scales are determined by the adhesion potential $V(z)$ and the bending rigidity. This leads to

$$\frac{F[z]}{k_\mathrm{B}T} = \sqrt{\kappa V_2 L_0^2} \int_S \left[\frac{1}{2}\left(\nabla^2 z\right)^2 + \frac{\Sigma}{2}\left(\nabla z\right)^2 + v(z)\right] \mathrm{d}^2\mathbf{r}, \tag{5.5$'$}$$

where

$$\Sigma = \frac{2\sigma L_0}{\sqrt{\kappa V_2}} = \frac{2R_0^2}{R_\mathrm{c}^2}, \tag{5.6}$$

$$R_0 = \left(\frac{\kappa L_0^2}{V_2}\right)^{1/4}. \tag{5.7}$$

We call R_0 the adhesion length (similar to the "persistence length" defined by Sackmann and Goennenwein (2006)), which turns out to control the interfacial width of the adhesion contact. In general $R_0 \sim 10$ nm $\ll R_\mathrm{c}$, therefore the surface tension term is unimportant.

We further notice that the combination $\sqrt{\kappa V_2 L_0^2}$ (even though L_0 is unspecified) controls the

magnitude of the free energy. If $\kappa V_2 L_0^2 \gg 1$, then the minima of $V(z)$ is separated by a large barrier (cf. Lipowsky (1995, 1994)). In this regime, thermal fluctuations are unimportant compared to the adhesion energy, and we can apply the mean-field capillary approximation.

5.2.2 Scaling analysis of the nucleation dynamics

Experimental measurements suggest that cell adhesion is a first-order transition (Albersdörfer et al., 1997; Boulbitch et al., 2001), therefore the potential minima are separated by a large barrier and adhesion should proceed via a nucleation-and-growth pathway. Here we study the nucleation dynamics in this regime using the classical capillary approximation.

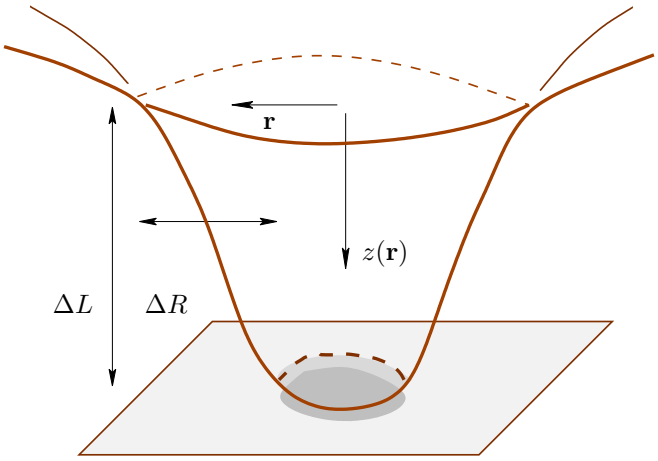

Figure 5.3: Illustration of a regular adhesion droplet

Initially the membrane is in a loosely bound state at a larger separation L_2, and the equilibrium shape is flat. Nucleation of an adhesion contact is driven by membrane undulations and results in a droplet as shown in Fig. 5.3. When thermal fluctuations are irrelevant, the boundary of the adhesion droplet is regular (a simple curve), and without loss of generality we assume the droplet to be axi-symmetric and the membrane deviation to be a function of the radius $z(r)$. If potential depths are comparable, i.e., $\Delta V \ll V_2$, the length scale L_0 associated with the adhesion potential $V(z)$ is naturally chosen to be the separation between the minima ΔL; otherwise when $\Delta V > V_2$, L_0 should be taken to be the separation of the metastable minimum (V_2) from the barrier, L_2.

In the first case, there is a well-defined adhesion "nucleus" which has size R in the interior and an interfacial area of width ΔR (cf. Fig. 5.3). The length scales are

$$L_0 = \Delta L,$$
$$R_0 = \left(\frac{\kappa \Delta L^2}{V_2}\right)^{1/4},$$

and the energy scale is

$$F_0 = \sqrt{\kappa V_2 \Delta L^2}.$$

From scaling analysis we have ($\Delta r = \Delta R/R_0, r = R/R_0$)

$$\nabla^2 z \sim \frac{L_0}{\Delta R^2}, \kappa \int (\nabla^2 z)^2 \mathrm{d}A \sim \frac{\kappa R L_0^2}{\Delta R^3}; \tag{5.8}$$

$$\int [V(z) - V(L_2)] \mathrm{d}A \sim -\pi R^2 \Delta V + \pi R \Delta R V_2. \tag{5.9}$$

Combining these two contributions we find

$$\Delta R \sim R_0 = \left(\frac{\kappa \Delta L^2}{V_2} \right)^{1/4}. \tag{5.10}$$

We recognize that the free energy is similar to that in the capillary approximation, with a line tension

$$\Gamma = \Delta R V_2 \sim \kappa^{1/4} V_2^{3/4} \Delta L^{1/2}. \tag{5.11}$$

At the critical radius $R^\ddagger$ the free energy attains maximum, and we have

$$R^\ddagger \sim \frac{V_2}{\Delta V} \Delta R = \frac{V_2}{\Delta V} \left(\frac{\kappa \Delta L^2}{V_2} \right)^{1/4} = \frac{V_2}{\Delta V} R_0, \tag{5.12}$$

$$F^\ddagger \sim \frac{V_2^2}{\Delta V} \Delta R^2 = \frac{V_2}{\Delta V} (\kappa V_2 \Delta L^2)^{1/2} = \frac{V_2}{\Delta V} F_0. \tag{5.13}$$

In the second case $V_2/\Delta V \lesssim 1$, and the radius R is comparable to the boundary width δR. The above results become

$$R \sim \delta R \sim R_0 = \left(\frac{\kappa \Delta L^2}{V_2} \right)^{1/4}, \tag{5.12$'$}$$

$$F \sim \pi R_0^2 V_2 = F_0. \tag{5.13$'$}$$

From Eqs. (5.12), (5.13) and (5.12$'$), (5.13$'$) we see that R_0 and F_0 control the length (R and ΔR) and energy (F) scales. The scaling $R^\ddagger \sim V_2^{-1/4}$ is different from classical mean-field results $R^\ddagger V^{-1/2}$ which is due to the difference in the surface energy. We note that the capillary analysis is valid only if $F_0 \gg k_\mathrm{B} T$, and thermal fluctuations are not important. In particular,

$$\kappa V_2 \Delta L^2 \approx 1 \tag{5.14}$$

marks the tricritical point where the unbinding transiton crosses over from first order to second order (Lipowsky, 1994).

5.2.3 Minimum-energy-path calculation

Under the mean field approximation (zero temperature limit), nucleation proceeds along the "minimum energy path," or the valley on the free energy landscape. We parametrize this path by a variable s and represent the path as

$$z(r,s) : s \to z(r).$$

The minimum energy path (MEP) is defined such that the tangent along the path $\nabla_s z(r,s)$ is parallel to the free energy gradient $\delta F[z]/\delta z$ at $z(r,s)$ for any s, or equivalently

$$\left(\frac{\delta F[z]}{\delta z}\right)^{\perp} = \frac{\delta F[z]}{\delta z} \cdot (\mathbf{I} - \hat{s}\hat{s}) = 0 \tag{5.15}$$
$$\hat{s} = \frac{\nabla_s z(r,s)}{\|\nabla_s z(r,s)\|}.$$

To calculate $z(r,s)$ we adopt the string method by E and co-workers (E et al., 2002), which is a modified steepest descent

$$\frac{\partial z(R,s;t)}{\partial t} = -\frac{\delta F[z]}{\delta z} \cdot (I - \hat{s}\hat{s}) + \lambda \hat{s}. \tag{5.16}$$

Here λ is a Lagrangian multiplier which is used to fix the parametrization s. The choice of λ is arbitrary, and we adopt the same parametrization as given by E et al. (2002), which requires the points be uniformly separated along the path,

$$\|\nabla_s z(r,s)\| = \text{const.}$$

which has a close form expression.

$\delta F[z]/\delta z$ is the free energy gradient

$$\frac{\delta F[z]}{\delta z} = \Delta^2 z - \Sigma \Delta z + v'(z). \tag{5.17}$$

In radial coordinates, the Laplacian is

$$\Delta \to \frac{\mathrm{d}^2}{\mathrm{d}r^2} + \frac{1}{r}\frac{\mathrm{d}}{\mathrm{d}r},$$

and

$$\Delta^2 \to \frac{\mathrm{d}^4}{\mathrm{d}r^4} + \frac{2}{r}\frac{\mathrm{d}^3}{\mathrm{d}r^3} - \frac{1}{r^2}\frac{\mathrm{d}^2}{\mathrm{d}r^2} + \frac{1}{r^3}\frac{\mathrm{d}}{\mathrm{d}r}.$$

To implement the steepest descent as described by Eq. (5.16), we proceed as follows: First we impose a circular droplet centered at $z = \Delta L$ which has a radius large enough such that letting it evolve along the free energy gradient (steepest descent) the size of the droplet grows instead of shrinking to the flat profile. After evolving for some steps the profile reaches steady growth, and

has passed the nucleation barrier, and this profile is taken as the final state $z(r, s = 1; t = 0)$, and the initial path is generated by a simple linear interpolation between $z = 0$ and $z(r, s = 1; t = 0)$. Although the final state $z(r, s = 1; t = 0)$ might not be on the minimum energy path, after iteration using Eq. (5.16), the whole path will evolve to the MEP and the maximum of the free energy corresponds to the critical "nucleus."

We adopt an explicit forward time splitting for the potential $V(z)$ and an implicit splitting for the differential operators, which ensures fast convergence[4]. Iteration stops when the maximum free energy of the reaction path $\max_s F[z(s)]$ reaches a constant and the maximum residual gradient $\max_s\{\nabla F(z)^\perp\}$ is used to test the accuracy of convergence. In the next section we discuss the numerical results.

5.3 Numerical results and discussion

In this section we discuss numerical results of the minimum-energy-path (MEP) calculations. Before the discussion we first estimate the typical length and energy scales associated with the adhesion process. The bending rigidity κ is about 20 $k_{\rm B}T$ for bilayer membranes and 1000 $k_{\rm B}T$ for cell membranes with actin cortices (Sackmann and Goennenwein, 2006; Bruinsma and Sackmann, 2002). The separation ΔL is between 5 and 50 nm, depending on the size of the receptors (Bruinsma et al., 2000; Martin et al., 2006), and we take $L_0 = 5$ nm. The barrier height V_2 is estimated to be 10^{-5} J/m^2 (Bruinsma et al., 2000). Therefore the energy scale for flexible membranes is (at $T = 300$ K)

$$F_0 = (\kappa V_2 \Delta L^2)^{1/2} \approx 1 k_{\rm B}T,$$

which indeed reflects flexibility. The lateral length scale is

$$R_0 = \sqrt[4]{\kappa \Delta L^2 / V_2} \approx 2 \text{ nm}.$$

In the case of cell membranes with actin network, F_0 increases by about 7 times and R_0 about 2.5 times. The capillary length

$$R_{\rm c} = \sqrt{\kappa/\sigma}$$

is usually of order 0.1μm (Sackmann and Goennenwein, 2006), and hence the surface tension

$$\Sigma \sim \frac{R_0^2}{R_c^2}$$

is small, and we neglect the surface tension term in our calculations except in the discussion of their effects on adhesion.

[4]See for example, the (p)reprints at `http://www.math.utah.edu/~eyre/research/methods/papers.html`.

In the following discussions quantities are represented using the scaled units. The scaled potential $V(z)$ is parametrized by the positions of the potential minima and their depth as

$$V(z) = p(z; -L_1, V_1) + p(z; L_2, V_2),$$

where $p(x; L, V)$ is given by

$$p(x; L, V) = -V\left[\left(\frac{x}{L} - 1\right)^2 - 1\right] \exp\left[-4\left(\frac{x}{L} - 1\right)^2\right]. \tag{5.18}$$

The combined potential has two minima located at $-L_1$ and L_2 with depths V_1 and V_2, and the barrier is located at $z = 0$. An example is shown in Fig. 5.4.

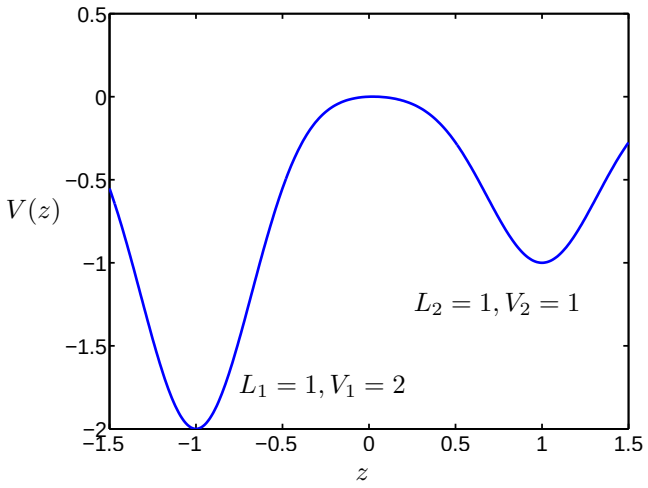

Figure 5.4: Shape of the potential $V(z)$ for $L_1 = L_2 = 1$, $V_1 = 2$, $V_2 = 1$

In Fig. 5.5 we present two representative nucleation paths. The barrier height is $V_2 = 1$, the locations of minima are $L_2 = 1$, $L_1 = 1$, and we choose two cases $V_1 = 1.3$ and $V_1 = 4$, giving potential depth difference $\Delta V = 0.3$ and 3, respectively. Figure 5.5(a) and (c) show the evolution of membrane shapes along the minimum energy path (MEP): the membrane conformation evolves in the direction of the arrow; Figure 5.5(b) and (d) give the free energy along the MEP with red circles corresponding to each membrane shape shown on the left. The red thick curves in (a) and (c) are the critical shape corresponding to the maximum free energy along the nucleation contour (saddle point).

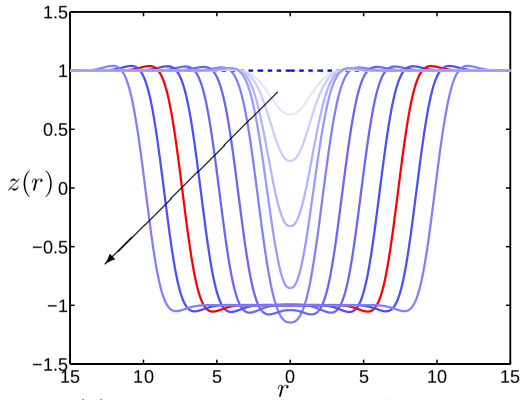

(a) Membrane shapes for $\Delta V = 0.3$

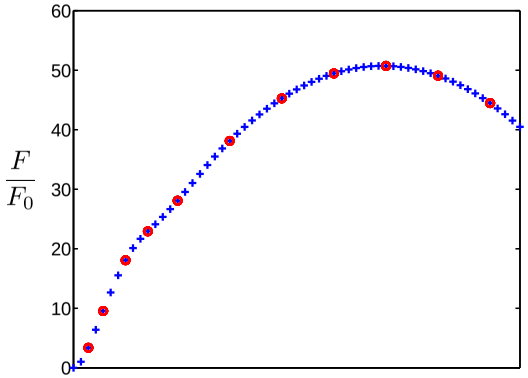

(b) Minimum energy path for $\Delta V = 0.3$

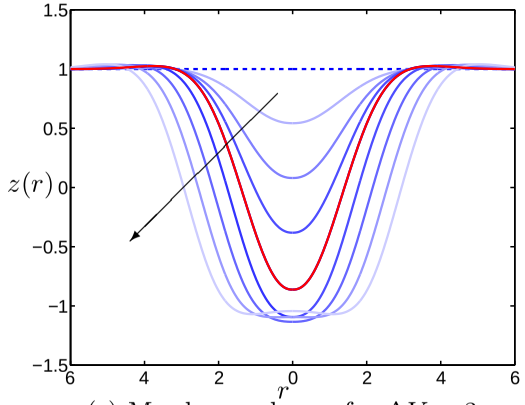

(c) Membrane shapes for $\Delta V = 3$

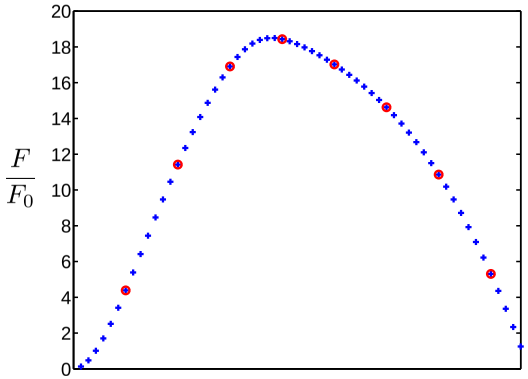

(d) Minimum energy path for $\Delta V = 3$

Figure 5.5: Evolution of the adhesion shape [(a) and (c)] and the free energy [(c) and (d)] along the minimum energy path for different adhesion potentials. Free energies of the representative shapes in (a) and (c) are shown as red circles in (b) and (d), with the red (most saturated) curve giving the critical shape corresponding to the maximum free energy along the contour. (a) and (b) are for the case when the potential depths are comparable, $V_1 = -1$ and $V_2 = -1.3$; (c) and (d) are for $V_1 = -1$ and $V_2 = -4$. In both cases the separation of the potential minima to the barrier is 1, given $\Delta L = 2$.

In the case that the barrier height is large, $\Delta V = 0.3 < V_2 = 1$, we see that the critical nucleus has a well-formed adhesion contact with radius $R^\ddagger \approx 7R_0 = 14$ nm, with an interfacial width $\delta R \approx 3R_0 = 6$ nm: this is similar to the classical nucleation scenario where capillary approximation applies. On the other hand for $\Delta V = 3 > V_2$, the critical shape has not formed an adhesion contact yet, but barely passed the barrier position $z = 0$. The free energy barrier in the second case is about 18 $k_\mathrm{B}T$ while in the first case is 51 $k_\mathrm{B}T$, the ratio is about 2.8, which is quite close to the scaling result given by $V_2/\Delta V = 1/0.3 \approx 3.33$.

To have a better understanding of the nucleation dynamics, we estimate the characteristic time scales of membrane undulations. By dimensional analysis, we have

$$\tau_\mathrm{un} \sim \eta L^3/k_\mathrm{B}T = 0.24 \text{ ns}$$

for $L = 1$ nm. For an energy barrier of 25 $k_\mathrm{B}T$ the nucleation time is

$$\tau_0 \sim \tau_\mathrm{un} e^{-F^\ddagger/kT} \sim 14 \text{ s}.$$

Therefore in the first case ($\Delta V = 3$) there is little barrier and nucleation is fast, while in the second case ($\Delta V = 0.3$) the nucleation barrier is so high that it is essentially impossible. It has been pointed out by Bruinsma et al. (2000) and by us (Martin et al., 2006) that in the initial stage of adhesion receptors form local aggregrates with very high densities, resulting in a deep potential minimum; our calculations further corroborate this assumption. On the other hand, for cellular adhesion the nucleation barrier is much higher and the reorganization of the actin cortex provides a mechanism to fortify the adhesion contact; other mechanisms such as dimerization can also be triggered by cell signaling.

Komura and Andelman (2000) studied the membrane shape near the phase boundary under lateral phase separation induced by adhesion, and found that the membrane deformation is non-monotonic near the phase boundary between coexisting phases. Our results show that this non-monotonic feature is present throughout the adhesion process. As we shall see at the end of this section, this feature is due to the bending energy term; increasing surface tension will diminish this feature.

To study the crossover between the two scenarios shown in Fig. 5.5, we plot the critical membrane shapes for different ΔV in Fig. 5.6. We notice that for $2 \leq \Delta V \leq 4$ the critical shape is almost invariant: in this regime the barrier height V_2 is small compared to the potential depth difference ΔV, and nucleation is determined by the potential near the metastable minimum at L_2. On the other hand, when ΔV is small, the critical shape has a well-developed adhesion contact with increasing radii as ΔV becomes smaller, and one can compare the critical radius and free energy with scaling results from the capillary approximation.

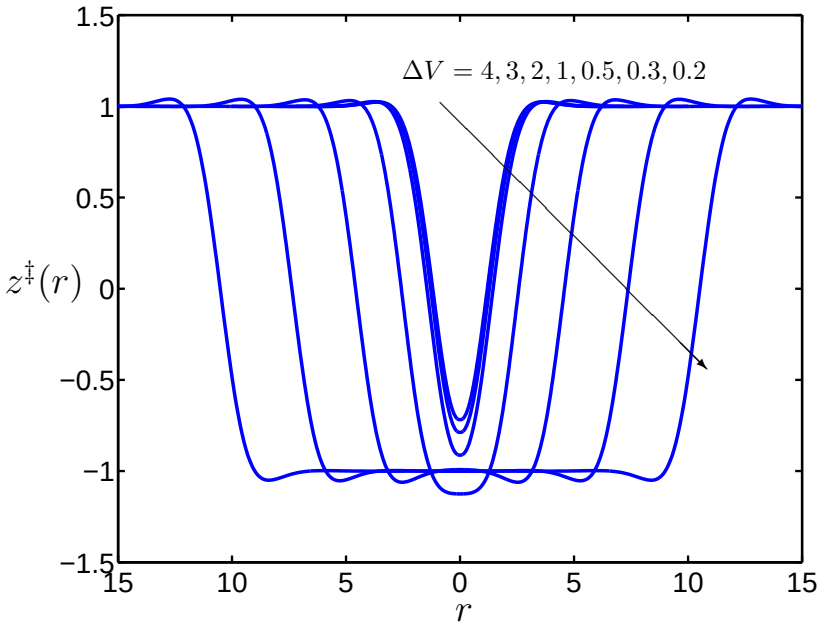

Figure 5.6: Critical membrane shapes at different potential depths. The positions of the minima are the same as in Fig. 5.5, $L_1 = L_2 = 1$. $V_2 = 1$ and $V_1 = V_2 + \Delta V$ with $\Delta V = 4, 3, 2, 1, 0.5, 0.3, 0.2$ along the arrow.

In Fig. 5.7 we plot the free energy barrier $F^{\ddagger}$ (maximum on the MEP) and the critical nucleus $R^{\ddagger}$, defined as the radius of the membrane contact within the adhesion minimum (with $z(r) < 0$). The plot is on a log-log scale. Scaling arguments imply that when $\Delta V \ll V_2$, the free energy barrier and the critical nucleus both scale as $1/\Delta V$. Numerical results indeed confirm this scaling. When $\Delta V \gg V_2$, scaling arguments suggest that ΔV is irrelevant, this trend also holds approximately.

Inspecting Fig. 5.6 we notice that critical shapes at different ΔV resemble the growth of a single adhesion contact, as in Fig. 5.5(a). Scaling analysis suggests that in the bending dominant regime the controlling length scale is $R_0 = (\kappa L_0^2/V_2)^{1/4}$, which is independent of the potential depth difference; in particular, the interfacial width $\delta R \sim R_0$. Therefore all membrane shapes look similar. Since only R_0 controls the shape of membrane deformations, we expect that the nucleation path in the conformation space is mostly determined by R_0, through the barrier height V_2, the length scale L_0 (which is proportional to ΔL here) and the bending rigidity κ; potential depth difference ΔV controls only the location of the saddle point along the nucleation path and the energy barrier.

To verify the dependence of nucleation on the minimum separation ΔL, we calculate the energy barrier $F^{\ddagger}$ and the critical radius $R^{\ddagger}$ for interacting potential $V(z)$ with potential minima having the same depths but varying locations. These results are shown in Fig. 5.8. The potential depths are fixed at $V_1 = 2$ and $V_2 = 1$ and the minima are located at $-L$ and L with L varying from 1 to 2. We see that scaling relations $R^{\ddagger} \propto \Delta L^{1/2}$ and $F^{\ddagger} \propto \Delta L$ fit well with numerical results.

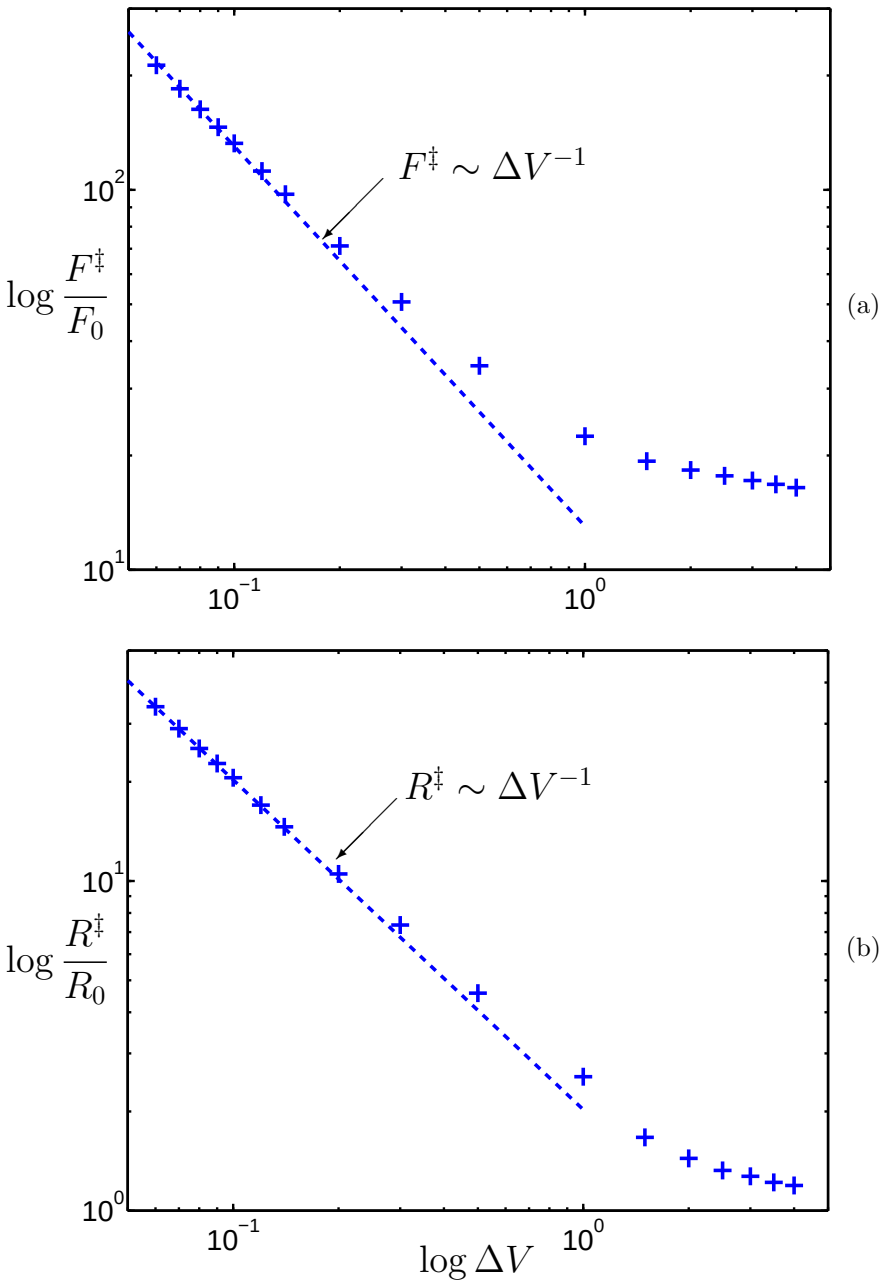

Figure 5.7: The saddle point free energy $F^\ddagger$ and the critical shape radius $R^\ddagger$ at different potential depths. The potential is identical to that in Fig. 5.6 with changing ΔV. The radius R is defined as the radial size of the contact area within the adhesion potential well: in our case the barrier is fixed at $z = 0$, therefore the radius is given by the size of the contact with $z \leq 0$.

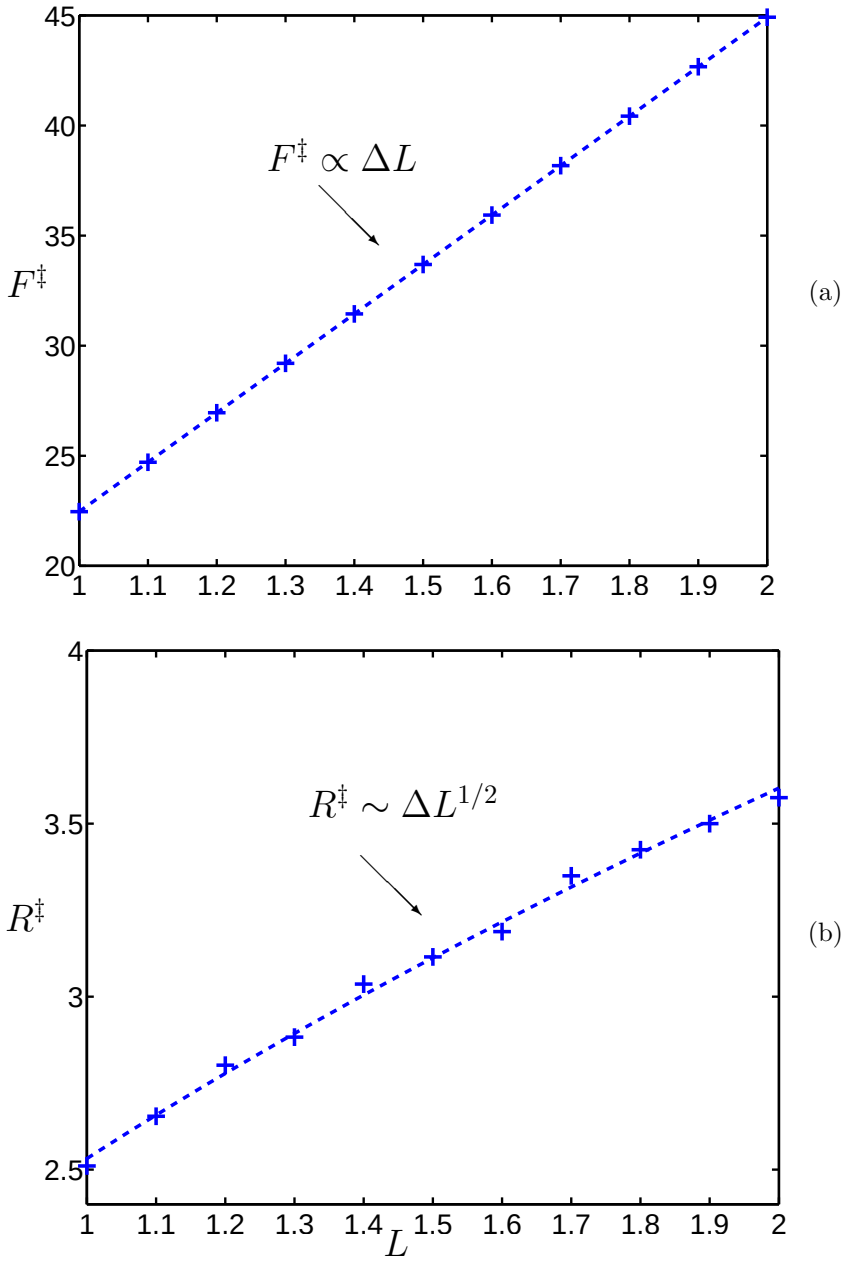

Figure 5.8: The saddle point free energy $F^\ddagger$ and the critical shape radius $R^\ddagger$ at different potential well separations. The potential wells are symmetrically positioned across the barrier with separation $\Delta L = 2L$ ranging from 2 to 4. The potential depths are fixed at $V_1 = 2$, $V_2 = 1$. Linear fits are done for $F^\ddagger$ against ΔL and $\log R^\ddagger$ against $\log \Delta L$ and show as dash lines.

Finally we study the effects of the surface tension term. Fig. 5.9(a) shows the development of an adhesion nucleus under strong surface tension $\Sigma = 3$. The potential depths are $V_1 = 2$ and $V_2 = 1$ and the minima are located at $L_1 = L_2 = 1$. Compared to the case with no surface tension, we observe that the membrane shape is flatter, and the extra surface energy increases the critical nucleus size. Fig. 5.9(b) shows the crossover of the critical membrane shape from rigidity-dominant regime to tension-dominant regime and the straighten-up of the membrane shape due to surface tension is apparent. In Fig. 5.9(c) we plot the energy barrier against the surface tension. Under a small surface tension, the size of the critical nucleus does not change much and is still determined by the adhesion length R_0, hence the extra surface area of the adhesion droplet is almost constant, and the free energy should be a linear function of the surface tension: this is also verified by numerical results.

In summary we have shown that the adhesion strength $R_0 = (\kappa \Delta L^2/V_2)^{1/4}$ controls the evolution of the membrane shape in the nucleation process, and the energy scale $F_0 = \sqrt{\kappa V_2 \Delta L^2}$ determines the nucleation barrier and the dynamics of the process. Our numerical results verify the scaling relations obtained from capillary approximations. In addition, the surface tension term flattens out the membrane shape and adds a surface energy to the energy barrier which is a linear function of the surface tension.

Our results apply to membrane adhesions mediated by any double-well adhesion potential. In particular, we note that our model also applies to the formation of the immunological synapse, which are focal contacts between a T-lymphocyte cell and an antigen-present cell (APC) (Grakoui et al., 1999). The synapse primarily consists of the T-cell receptor (TCR)–Major Histocompatibility molecule-peptide Complex (MHC) bonds and integrin (ICAM-1/LFA-1) bonds. Due to their different spatial extensions (the natural size of the integrin-ligand bond is $\sim$40nm, and is about 15nm for the TCR-MHC complex), the binary system consisting of TCR and integrin binding should exhibit a double-well interaction potential (Raychaudhuri et al., 2003). Given the high membrane bending rigidity ($\sim 400kT$) of the T-cell, our results suggest that even after the integrin bonds form an adhesion contact (surfaces are brought close to 40nm separation), nucleation of the TCR contact at normal TCR densities still exhibits a considerable barrier. Such a barrier would be impossible to overcome by thermal fluctuations. Therefore some active mechanism is likely to be involved that overcomes this barrier. Alternatively, increasing TCR expression could lower the TCR binding minimum, thereby descreasing the nucleation barrier [cf. Fig. 5.7(a)], which is the case in the synapse between a mature T-cell and APC (Qi et al., 2001). The fact that the synapses between premature T-cells (thymocytes) and the APC do not show a well-developed contact with TCR-MHC bonds could be due to either insufficient TCR bonds (Lee et al., 2003; Raychaudhuri et al., 2003), or the absence of active mechanisms to overcome the high energy barrier. Our calculations thus offer a complementary perspective to the work by Chakraborty and co-workers which did not explicitly

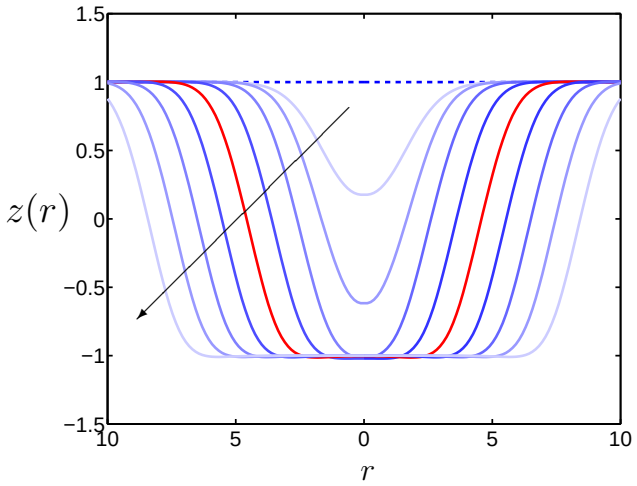

(a) Evolution of the membrane shape with $\Sigma = 3$

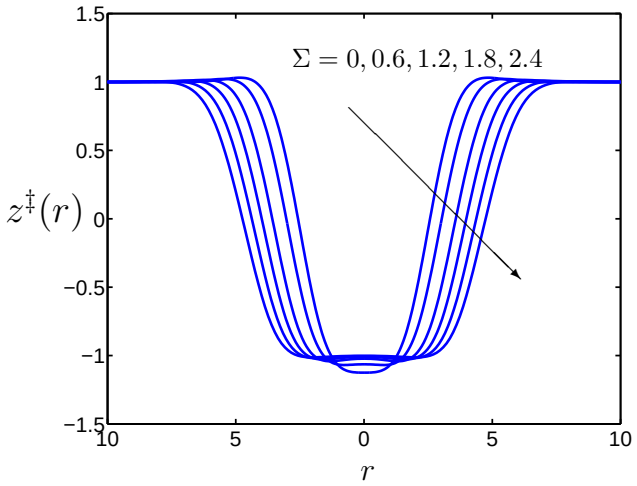

(b) Critical membrane shapes at different Σ

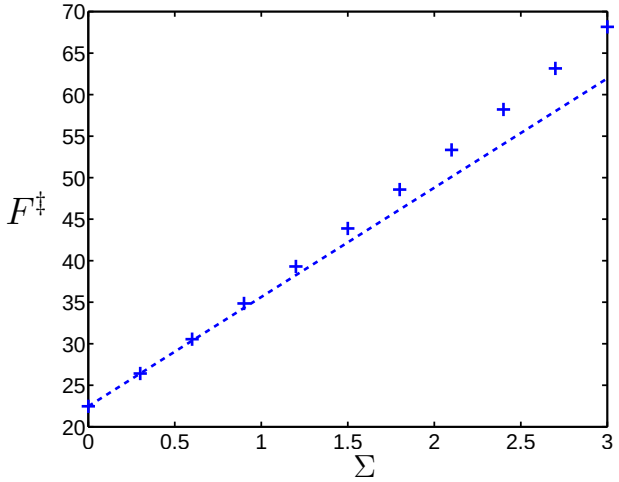

(c) Saddle point free energy at different Σ

Figure 5.9: Illustration of the effects of surface tension. The potential is parametrized by $L_1 = L_2 = 1$, $V_1 = -2$, $V_2 = 1$.

address the issue of nucleation.

5.4 The Peierls argument near the critical unbinding transition

Above we have discussed the nucleation dynamics of adhesion that is controlled by a large energy barrier. Here we study the scenario when the energy barrier is small, i.e.,

$$\kappa V_2 L_0^2 \lesssim k_{\rm B}T.$$

This is the case when the barrier is small or the membrane is very flexible. In this regime thermal fluctuations (membrane undulations) are comparable to the size of adhesion plaques, and the shape of the adhesion contact may be irregular. Our discussions follow those by Lipowsky and co-workers (Lipowsky, 1994, 1995; Lipowsky and Dimova, 2003).

Before the discussion of adhesion dynamics we first briefly discuss the interaction between the membrane surfaces due to shape undulations. For a membrane confined within a well of width W, the confinement free energy is found to be (Lipowsky, 1995)

$$\frac{V}{k_{\rm B}T} = \frac{c_1}{\kappa W^2}. \tag{5.19}$$

c_1 is a constant of order 1. This extra entropic repulsion contributes to the free energy at each minimum $c_1/\kappa W^2$, and results in an effective energy barrier $V_{\rm eff} < V_2$, the bare energy barrier that is calculated based on molecular models of ligand-receptor binding by us (Martin et al., 2006).

Taking into account the entropic contributions, we find the renormalized potential depth difference ΔV to be

$$\Delta V = \Delta V_{\rm bare} - \frac{c_1}{\kappa W_1^2} + \frac{c_1}{\kappa W_2^2}, \tag{5.20}$$

where $W_{\rm i}$ are the widths of the potential minima. $\Delta V = 0$ corresponds to the binodal phase coexistence (binding-unbinding transition).

If κ is small or the energy scale $F_0 = \sqrt{\kappa V_{\rm eff} L_0^2} \sim k_{\rm B}T$, then membrane undulations are prominent and the boundary width δR is controlled by thermal fluctuations and determined as

$$\kappa \left(\frac{L_0}{\delta R^2}\right)^2 \delta R^2 \sim 1 \Rightarrow \delta R \sim \sqrt{\kappa} L_0. \tag{5.21}$$

Here L_0 is the membrane roughness which measures the magnitude of thermal undulations. In the adhesion we can take L_0 to be the width of the metastable minimum W_2.

As we mentioned at the beginning of this section, membrane undulations induce an effective

repulsion between the surfaces; the effective barrier height is

$$V_{\rm eff} = V_2 - \frac{c_1}{\kappa W_2^2}, \tag{5.22}$$

where the 2nd term corresponds to the confinement energy of membrane undulations within the metastable minimum. The line tension is given by

$$\gamma \propto V_{\rm eff}\delta R. \tag{5.23}$$

If $\kappa V_2 W_2^2 \lesssim k_{\rm B}T$, then the line tension becomes zero and the barrier vanishes. Below we focus on the case when $\kappa V_2 W_2^2 > k_{\rm B}T$ with $V_{\rm eff} > 0$.

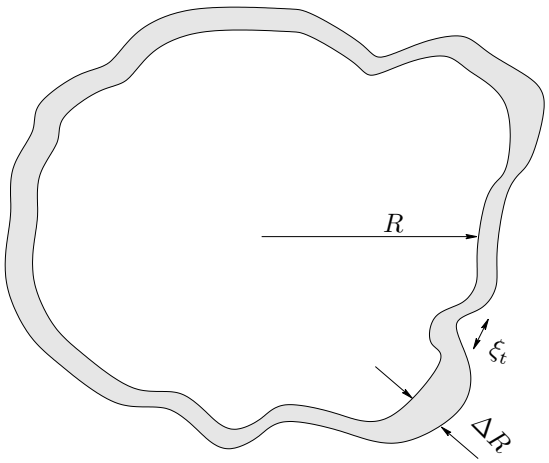

Figure 5.10: Projection of an irregular droplet

When fluctuations are prevalent, the domain boundaries between the adhesion states (corresponding to the two potential minima) are irregular, and we can apply a Peierls-type argument to account for the extra entropic contribution due to the fluctuations of the boundary shapes. Assume the boundary to be a self-avoiding walk in 2D plane (2D SAW) with Hausdorff dimension 4/3, then the perimeter of a droplet scales as

$$\mathcal{L} \sim \frac{R^{4/3}}{\xi_{\rm t}^{1/3}}, \tag{5.24}$$

where $\xi_{\rm t}$ is the "unit" step size of this self-avoiding loop (δR is the width of this loop, see Fig. 5.10). The configuration entropy of the domain boundary is given by

$$S \approx c_2 \frac{\mathcal{L}}{\xi_{\rm t}}, \tag{5.25}$$

c_2 is a universal constant.

For a string with line tension γ and width δR, the step size or persistence length scales as

$\xi_t \sim \gamma\delta R^2$, therefore the combined interface energy is given by

$$\begin{aligned}\Gamma = \gamma\mathcal{L} - S &= \left(\gamma - \frac{c_2}{\xi_t}\right)\mathcal{L} \\ &= \left(\gamma - \frac{c_2}{\gamma\delta R^2}\right)\frac{R^{4/3}}{(\gamma\delta R^2)^{1/3}}.\end{aligned} \tag{5.26}$$

We see that if $\gamma\delta R \sim 1$, i.e.,

$$\kappa V_{\text{eff}} L_0^2 \sim 1, \tag{5.27}$$

then the interface energy is of order $k_B T$ and adhesion is a second-order transition. If $\gamma\delta R \gg 1$, then

$$\Gamma \sim V_{\text{eff}}^{2/3} R^{4/3}, \tag{5.28}$$

and adhesion is a weak first-order transition. While Eq. (5.27) gives the transition from first order adhesion to second order, which should be governed by a tricritical point (Lipowsky, 1995).

For the weak first order transition that is still governed by the critical point, we can modify the capillary argument by incorporating the entropic correction. For an adhesion plaque ("nucleus"), the total free energy is

$$\begin{aligned}F &= -\pi R^2 \Delta V + \Gamma, \\ &= -\pi R^2 \Delta V + R^{4/3} V_{\text{eff}}^{2/3}.\end{aligned} \tag{5.29}$$

The critical radius is

$$R^{\ddagger} \sim V_{\text{eff}} \Delta V^{-3/2}, \tag{5.30}$$

and the free energy barrier scales as

$$F^{\ddagger} \sim \left(\frac{V_{\text{eff}}}{\Delta V}\right)^2. \tag{5.31}$$

Eqs. (5.30) and (5.31) apply to the regime when the persistence length of the boundary $\xi_t \ll R$, i.e,

$$\gamma\delta R^2 \ll R^{\ddagger} \Rightarrow \kappa \Delta V L_0^2 \ll 1. \tag{5.32}$$

This is further translated into $\Delta V \ll V_{\text{eff}}$. We note that in this regime the critical size $R^{\ddagger}$ and the energy barrier only depend on the potential depths, but not on the length scale associated with the potential $V(z)$; this is because membrane undulations are comparable to the separation between the potential minima, and the tunneling of the barrier is controlled by thermal fluctuations but not the shape of the adhesion potential.

If $\kappa\Delta V L_0^2 > \kappa V_{\text{eff}} L_0^2$, then

$$R \sim \delta R = \sqrt{\kappa} L_0 \tag{5.30$'$}$$

and the energy is given by

$$F \sim R^2 V_{\text{eff}} = \kappa V_{\text{eff}} L_0^2. \tag{5.31'}$$

Table 5.1 summarizes the scaling results in this section and in Section 5.2.2.

Rigid Membrane $\kappa V_2 L_0^2 \gg 1$		
	$V_2 \gg \Delta V$	$\Delta V \gtrsim V_2$
R	$\frac{V_2}{\Delta V}\left(\frac{\kappa \Delta L^2}{V_2}\right)^{1/4}$	$\left(\frac{\kappa L_2^2}{V_2}\right)^{1/4}$
F	$\frac{V_2}{\Delta V}\sqrt{\kappa V_2 \Delta L^2}$	$\sqrt{\kappa V_2 L_2^2}$
Flexible membrane $\kappa V_{\text{eff}} L_0^2 \gtrsim 1$		
	$V_{\text{eff}} \gg \Delta V$	$\Delta V \gtrsim V_{\text{eff}}$
R	$V_{\text{eff}}/\Delta V^{3/2}$	$\sqrt{\kappa} W_2$
F	$(V_{\text{eff}}/\Delta V)^2$	$\kappa V_2 W_2^2$

Table 5.1: Summary of scaling results

5.5 Conclusion

In this paper we have systematically studied the nucleation dynamics of membrane adhesions mediated by specific receptor binding. We distinguish between the different regimes according to the nature of the adhesion and the shape of the adhesion potential. Scaling arguments suggest that in the rigid-membrane regime when adhesion is a first-order transition, the geometry of the membrane shape is controlled by the adhesion length R_0, while the energetics is controlled by the characteristic energy $F_0 = \sqrt{\kappa V_2 L_0^2}$ —where L_0 is the length scale associated with the adhesion potential, V_2 is the barrier height, and κ is the bending rigidity. These conclusions are further verified from our numerical calculations of the minimum energy path.

When the membrane is very flexible or the barrier is small, entropic effects due to membrane undulations are important, and adhesion is a weak first-order transition controlled by the characteristic energy scale given by $F_0 = \sqrt{\kappa V_{\text{eff}} L_0^2}$. If the potential depth difference ΔV is small, the adhesion droplet still has a well-defined but irregular boundary. Applying a Peierls argument we find that the nucleation dynamics depend on the geometric dimension of the boundary of the adhesion droplet. In addition, the energy barrier and the critical nucleus size only depend on the potential depths but not their locations.

The surface tension term increases the nucleation barrier as well as the size of the critical nucleus. But we find that at a small surface tension, the shape of the nucleus is still controlled by the adhesion length R_0, which is almost unaffected by the surface tension, implying that the extra surface area

in the critical adhesion droplet is almost constant. We also show that the non-monotonic feature in the membrane shape near the phase boundary, as was first found by Komura and Andelman (2000), is due to the bending energy term and is reduced at increasing surface tension.